Recibido: 31/01/2019
Aceptado: 27/05/2019

REVISTA DE TELEDETECCIÓN
Asociación Española de Teledetección
2019 53, 17-32
ISSN 1133-0953
EISSN 1988-8740
https://doi.org/10.4995/raet.2019.11320

Methods for tree cover extraction from high resolution orthophotos and airborne LiDAR scanning in Spanish *dehesas*

Borlaf-Mena, I.[1*], Tanase, M.A.[1], Gómez-Sal, A.[2]

[1] *Department of Geology, Geography and Environment, Faculty of Biology, Chemistry and Environmental Sciences, University of Alcalá, Alcala de Henares, Spain.*

[2] *Department of Life Sciences, Faculty of Biology, Chemistry and Environmental Sciences, University of Alcalá, Alcala de Henares, Spain.*

Abstract: *Dehesas* are high value agroecosystems that benefit from the effect tree cover has on pastures. Such effect occurs when tree cover is incomplete and homogeneous. Tree cover may be characterized from field data or through visual interpretation of remote sensing data, both time-consuming tasks. An alternative is the extraction of tree cover from aerial imagery using automated methods, on spectral derivate products (i.e. NDVI) or LiDAR point clouds. This study focuses on assessing and comparing methods for tree cover estimation from high resolution orthophotos and airborne laser scanning (ALS). RGB image processing based on thresholding of the 'Excess Green minus Excess Red' index with the Otsu method produced acceptable results (80%), lower than that obtained by thresholding the digital canopy model obtained from the ALS data (87%) or when combining RGB and LiDAR data (87.5%). The RGB information was found to be useful for tree delineation, although very vulnerable to confusion with the grass or shrubs. The ALS based extraction suffered for less confusion as it differentiated between trees and the remaining vegetation using the height. These results show that analysis of historical orthophotographs may be successfully used to evaluate the effects of management changes while LiDAR data may provide a substantial increase in the accuracy for the latter period. Combining RGB and Lidar data did not result in significant improvements over using LIDAR data alone.

Key words: Low-density airborne Lidar, PNOA, Tree cover, *Quercus ilex*.

Métodos para la estimación de la cabida cubierta a partir de ortofotografías de alta resolución y LiDAR aeroportado en dehesas españolas

Resumen: Las dehesas son agroecosistemas de alto valor que se benefician del efecto de la cobertura arbórea sobre el pasto. Este efecto facilitador aparece cuando la cobertura arbolada es incompleta y homogénea. La cobertura arbórea puede caracterizarse con datos de campo o mediante fotointerpretación de datos de teledetección, ambas tareas que requieren mucho tiempo. Una alternativa es extraer la cobertura arbórea a partir de imagen aérea, derivados espectrales (i.e. NDVI) o nubes de puntos LiDAR. Este estudio se centra en evaluar y comparar métodos para la estimación de cobertura arbolada a partir de ortofotografías de alta resolución y LiDAR aeroportado (ALS).

To cite this article: Borlaf-Mena, I., Tanase, M.A., Gómez-Sal, A. 2019. Methods for tree cover extraction from high resolution orthophotos and airborne lidar scanning in Spanish *dehesas*. *Revista de Teledetección,* 53, 17-32. https://doi.org/10.4995/raet.2019.11320

* *Corresponding author: ignacio.borlaf@gmail.com*

El procesado de imagen RGB basado en la umbralización del índice 'Excess green minus excess red' con el método de Otsu produjo resultados aceptables, algo peores que los obtenidos mediante umbralización del modelo digital de copa obtenido con datos ALS (87%) o al combinar datos RGB y LiDAR (87.5%). La información RGB resultó ser útil para la delineación de copas, aunque muy vulnerable a la confusión con pastos o arbustos. La extracción basada en ALS sufrió menos confusión, ya que diferencia entre el arbolado y otros tipos de vegetación usando la altura. Estos resultados muestran que el análisis de ortofotografías históricas podría usarse para evaluar el efecto en los cambios en la gestión, mientras que los datos LiDAR pueden permitir un aumento sustancial en la precisión en períodos posteriores. Combinar LiDAR y RGB no produjo una mejora sustancial sobre el uso de datos LiDAR.

Palabras clave: LiDAR aeroportado de baja densidad, PNOA, fracción de cabida cubierta, *Quercus ilex*.

1. Introduction

Dehesas are agroforestry systems established in tracts of land where soil is unfit for continuous cultivation and are typical to the Mediterranean climate region of Iberian Peninsula. They are characterized by scattered trees, generally evergreen oaks, which represent a low fraction of the total vegetation cover (21-40%, Moreno and Pulido, 2009), and have an homogeneous distribution. Such arrangement avoids inter-tree competition, enhances tree productivity, and facilitates the growth of pastures (De Miguel *et al.,* 2013). These effects aid the production role of these ecosystems, providing not only feed for both livestock and game species (their main use), but also other products like wood or cork (Moreno & Pulido, 2009).

Due to the dependence of *dehesas* functioning of tree cover and arrangement, their retrieval is essential for a sustainable management. The proportion of tree cover or fractional canopy cover (FCC) is defined as 'proportion of ground covered by the vertical projection of the canopy' (Jennings *et al.,* 1999) . FCC can be estimated using different methods starting with visual observations or field ceptometers (White *et al.,* 2000). However, remote sensing is currently one of the most commonly used methods for FCC extraction with a detailed review on the different techniques available being found in Ke and Quackenbush (2011).

Techniques for FCC extraction may vary depending on the choice of sensor (resolution, active/passive, etc.). Approaches using high resolution sensors usually estimate the FCC based on the values of spectral bands or a derivate (i.e. spectral indices). Landsat 5 TM (Joffre & Lacaze, 1993; Pu *et al.,* 2003; Xu *et al.,* 2003; Carreiras *et al.,* 2006), SPOT 1 HRV (Joffre & Lacaze, 1993), Terra ASTER (Abbasi & Bakhtyari, 2012) and Sentinel-2 MSI (Godinho *et al.,* 2018) have been employed for tree cover mapping in low-density *Quercus* forests. In these studies a recurring source of reference is imagery with higher spatial resolution, using either manual (Joffre & Lacaze, 1993; Carreiras *et al.,* 2006; Godinho *et al.,* 2018) or automated methods for its extraction (Pu *et al.,* 2003; Xu *et al.,* 2003; Abbasi & Bakhtyari, 2012).

When using very high-resolution imagery (e.g., sub-meter), the focus generally shifts to tree cover delineation. Many of these studies focus on coniferous dominated forests where trees are easier to delineate when compared to deciduous species which are characterized by irregular canopy projections and illumination pattern (Ke & Quackenbush, 2011). Tree delineation in semiarid environments used pansharpened imagery from either Spot-5 (Boggs, 2010; Fisher *et al.,* 2016) or Quickbird satellites (Boggs, 2010; Lavado *et al.,* 2012). The techniques employed were based on thresholding of tree probability (Fisher *et al.,* 2016), the NDVI (Boggs, 2010) or object-based image analysis (OBIA) (Boggs, 2010; Lavado *et al.,* 2012).

In the Mediterranean basin, numerous authors used optical remote sensing to characterize the pattern of vegetation in *dehesas* (Romero de los Reyes *et al.,* 2007; Castillejo-González *et al.,* 2010; Lavado *et al.,* 2012). Some studies (Romero de los Reyes *et al.,* 2007; Castillejo-González *et al.,* 2010) used thresholding techniques for FCC extraction while others used object based image analysis (OBIA) (Lavado *et al.,* 2012).

Thresholding techniques were used with visible (Red, Green, and Blue -RGB bands) and panchromatic orthophotos (Romero de los Reyes *et al.,* 2007) , or a combination of visible and near infrared (NIR) bands acquired by very high resolution satellite sensors such as QuickBird (Castillejo-González *et al.,* 2010). OBIA was used with orthophotos acquired through the Spanish National Plan of Aerial Orthophotography (PNOA in its Spanish acronym) in 2009, as well as from the United States Army Map service (1956 and 1957) (Lavado *et al.,* 2012). The most useful band was the NIR (when multispectral imagery is available) or spectral indices including the NIR channel (Ke & Quackenbush, 2011). For example, Castillejo-González *et al.* (2010) used the Normalized Difference Vegetation Index (NDVI), along with the original bands to improve the results of the FCC classification. When only RGB imagery was available, the green band was usually selected for tree delineation (Ke & Quackenbush, 2011). An alternative to using the green band alone are spectral indices derived from RGB channels as formulated in the context of precision agriculture. Some examples are the Excess Green Index (EGI o ExG, depending on the author) (Woebbecke *et al.,* 1995), Excess Red (ExR) (Meyer *et al.,* 1999), Excess Green minus excess Red (ExGR) (Meyer & Neto, 2008) or the Color Index of Vegetation Extraction (CIVE) (Kataoka *et al.,* 2003).

Airborne lidar scanning (ALS) point clouds were also used to estimate the FCC. Some studies used the gap probability, the proportion of first returns divided by the total number of returns (Morsdorf *et al.,* 2006; Jones & Vaughan, 2010; García, 2011; Fisher *et al.,* 2016) to extract FCC related information. Other studies where based on creating a binary raster (tree *vs.* no tree) and then calculating the proportion of pixels classified as tree (García, 2011). The pre-classified raster was obtained by applying a condition of minimum height to the canopy height model (CHM). One study combined RGB orthophotos and ALS data where an RGB-based index is used for vegetation detection and an ALS based CHM is used to separate individual canopies through watershed segmentation (Chen *et al.,* 2005). Other studies used ALS in combination with multispectral aerial imagery containing the NIR channel (Mumtaz & Mooney, 2008; Dechesne *et al.,* 2016). These later studies were focused on land cover classification (As opposed to FCC extraction) with vegetation being one of the classes extracted.

The great opportunities provided by ALS for individual tree-crown detection have been highlighted in Ke and Quackenbush (2011) together with their main drawback, the prohibitive ALS acquisition costs. Over the past years, such drawbacks slowly disappeared with the growth of national ALS remote sensing programs offering open data access. One such example is the Spanish National Plan of Aerial Orthophotography (PNOA, in its Spanish acronym) which, since 2015, offers free access to the geographic information collected by the Spanish National Geographic Institute (IGN). PNOA systematically and periodically collects and makes available highly detailed spatial information (RGB orthophotos, low density ALS data, digital elevation models) with wall to wall coverage over the Spanish territory (IGN, 2014). Coupled with increasing availability of free and/or open software (Free Software Foundation, 2016) for data processing and analysis, such as FUSION (McGaughey, 2016), GRASS GIS (Neteler & Mitasova, 2008), QGIS (Quantum GIS Development Team, 2017), Orfeo Toolbox (Inglada & Christophe, 2009) or PDAL (Butler & Gerlek, 2017), PNOA data provides for an extraordinary opportunity to developing low cost applications calibrated and validated at regional to national levels.

In this context, the aim of this study was to develop and compare a series of automated methods for extracting FCC in *dehesas* using PNOA orthophotos and low-density ALS datasets. A secondary objective was testing the utility of different RGB indices and thresholding techniques, as to the authors knowledge, there is an information gap around their use for FCC extraction.

2. Study area and datasets

2.1. Study area

This study was carried out at 10 sites, representative of different *dehesas* groups as defined in the framework of the LIFE+ bioDehesa project. The sites are scattered around Andalusia region, mainly in Sierra Morena and Los Alcornocales ranges, and are generally linked to natural protected areas (Figure 1). Their code and main characteristics are shown in Table 1 (Gómez-Sal,

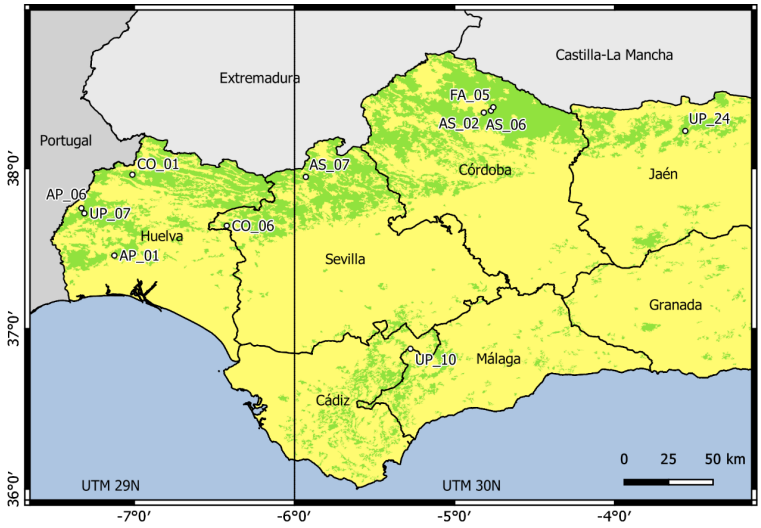

Figure 1. Sites location (points) over *dehesas* distribution (green shades) in Andalusia. (Junta de Andalucía, 2018).

2016). In all cases the dominant tree species was holm Oak (*Quercus ilex* L.).

2.2. Datasets

The remote sensing data used in this study were collected during 2013 (orthophotos of all sites) and 2014 (ALS flight). The only exception is the site UP 10, where the ALS dataset was collected during 2008 along with an orthophotography. All the datasets were available from IGN through a dedicated web-portal except for the ALS data for site UP 10 (acquired for a hydrological study) which were provided by the council of Andalusia. The reference system for all layers is ETRS89 with UTM projection (zones 29 and 30 North). Orthophotos were acquired with a photogrammetric camera with automatic exposition control. Each orthophoto consists of three channels (Red: R, Green: G, Blue: B) with 8-bits encoding and a pixel size of 50 cm, except for the site UP 10, where the pixel size is 45 cm. Orthophotos were collected on clear days between May and September, when the sun elevation over the horizon was above 40° (IGN, 2016). The PNOA ALS data was acquired with a maximum scan angle of ±50° (for most states scan angles are under 40°), at a scanning frequency of 70 Hz (minimum of 40 Hz), and a minimum pulse frequency of 45 kHz. The maximum flight height was 3000 m above ground level. The minimum point cloud density is 0.5 returns per square meter (maximum

Table 1. Information about the sites. The slope information has been extracted from the DEM. Cover information is reported as it appears in Gómez Sal *et al.* 2016

	Slope					
Code	P05	Average	P95	Tree cover	Shrub cover	Herbaceous cover
UP 10	10	32	60	Low	Medium/high	Low
CO 06	5	20	45	Medium	Very high	Low
AS 07	9	33	74	High	Medium	High
AP 06	5	15	26	Medium	Medium/low	High
AS 02	2	9	25	High	Medium/low	High
AS 06	2	5	10	Medium	Very low	Very high
FA 05	2	6	11	Low	Medium/low	Medium/high
UP 24	5	22	45	Low	Low/very low	High
CO 01	4	14	29	High	Medium/low	High
UP 07	2	8	17	High	Very Low	High

spacing between points of 1.41 m). The raw ALS data were processed with the TerraScan software (Soininen & TerraSolid, 2016) with the RMSE for height being below 20 cm (IGN, 2019).

3. Methods

FCC extraction was tested using three methods based on i) RGB images, ii) ALS data analysis and iii) RGB and ALS data combined. The results were validated against tree presence reference point layers through the percentages of accurate predictions, and omission/commission errors, as described in section 3.4. In the specific case of FCC extraction with RGB indices an additional layer was created through manual delineation of tree canopy cover areas to perform a detailed assessment of the effect of each operation. The software employed for processing the data were QGIS (Quantum GIS Development Team, 2017), GRASS GIS (Neteler & Mitasova, 2008), Python (Python Software Foundation, 2010) and the libraries Numpy (van der Walt *et al.,* 2011), Scipy (Jones *et al.,* 2014) and Scikit-Image (van der Walt *et al.,* 2014).

3.1. FCC extraction with RGB indices

Due to the variety of options that can be applied for the FCC extraction, different experiments were carried out to determine the optimal combination of indices, thresholds, and approaches. Several steps were needed including the selection on the optimal spectral index, the calculation of index specific thresholds, the selection of the segmentation approach, and post-processing to reduce noise and abnormal objects.

3.1.1. Reference layer and performance metrics for FCC extraction with RGB indices

To assess the effect of each algorithm, a reference canopy area layer was manually delineated (vector) over the orthophoto from 2013 of site CO 01. The crown of each tree (or groups of trees) was manually digitized using as background the RGB channels. The purpose of this layer was to help assessing the effect of each operation incorporated in the workflow (see section 3.1.6) employed for canopy delineation from RGB orthophotos.

In total, nine combinations (e.g., optical index-thresholding, method-segmentation approach) were evaluated to define the optimal workflow to extract FCC based on RGB imagery. The results of all these combinations were assessed against the reference tree cover by examining the overall accuracy, as well as the tree segments (i.e., clusters of pixels identified as 'tree') statistics (e.g., number, mean and median segment size).

3.1.2. Spectral index selection

The first step was determining which RGB-derived index was better suited for trees classification. ExG (Equation 3), ExR (Equation 4), ExGR (Equation 5), and CIVE (Equation 6) were analyzed. For comparability reasons, a single method, Otsu threshold (Otsu, 1979), was used to separate between vegetated and non-vegetated areas. The Otsu threshold assumes that image values have a binomial distribution, belonging to two classes. Based on this assumption, the algorithm looks for a threshold that separates the two classes so that the variance in each class is minimized. The computed threshold is then used to separate the classes. Its advantage resides in its capacity to account for different ranges of the spectral indices as opposed to merely using a fixed threshold (i.e. the 0 value). The spectral indices were calculated after the normalization of the digital raw numbers using the equations 1 and 2.

$$R^* = \frac{R}{R_{max}}; G^* = \frac{G}{G_{max}}; B^* = \frac{B}{B_{max}} \quad (1)$$

$$r = \frac{R^*}{R^* + G^* + B^*}$$

$$g = \frac{G^*}{R^* + G^* + B^*} \quad (2)$$

$$b = \frac{B^*}{R^* + G^* + B^*}$$

Where:

R, G and B are the values of the pixel on each band.

R_{max}, G_{max} and B_{max} are the maximum values of each band.

R^*, G^* and B^* are the normalized Red, Green, Blue values.

r, g and b are the proportion of each band to the total illumination.

After normalization, the spectral indices are were calculated as follows:

$$ExG = 2g - r - b \quad (3)$$

$$ExR = 1.4r - g \quad (4)$$

$$ExGR = ExG - ExR = 2g - r - b - (1.4r - g) = 3g - 2.4r - b \quad (5)$$

$$CIVE = 0.441r - 0.811g + 0.385b + 18.787 \quad (6)$$

The sensitivity of each index was evaluated calculating the overall classification accuracy as well as the statistics of the tree segments (size, number) as explained above, using the canopy area layer as a reference.

3.1.3. Threshold selection

The second step was focused on establishing the optimal thresholding method, by assessing the effect of different thresholds on the ExGR index (selected as the most suited for tree classification, see sections 3.1.2 and 4.1). Three thresholding options were compared:

i. A fixed value '0' indicates the 'Greenness' index is higher than the 'Redness' one (Meyer & Neto, 2008).

ii. The mean of the index considering all the pixels in the image (Guijarro *et al.,* 2011) was tested because it is expected to be dominated by the abundance of 'ground' pixels with low Greenness, whereas the trees will have a higher greenness value.

iii. The Otsu threshold (Otsu, 1979) (see section 3.1.2). It was tested under the reasoning that the image should contain two 'populations' of pixels with distinct values of 'Greenness' (tree/other).

The index value had to be equal or higher than the chosen threshold (i.e. 0) for a pixel to be classified as 'tree'. Threshold selection was based on the overall classification accuracy and the similarity of tree segments statistics to the canopy area reference layer.

3.1.4. Segmentation approach

Two types of segmentation approaches were tested: i) pixel-based, where every pixel must meet a specified threshold condition (i.e., higher value of ExGR than the Otsu threshold), and ii) region growing based, where the pixels are grouped into segments based on their similarity, and these segments must meet the same specified condition. The segmentation was applied after the optimization of segmentation (Lennert, 2016). The first parameter optimized was the similarity threshold, which defines the difference needed for not including a pixel in the segment. The selected values for this parameter (0.02, 0.05, 0.10, 0.15, 0.2 y 0.25) were obtained through preliminary trials. The second parameter optimized was the minimum segment size. We have chosen values of 5 and 13 pixels, roughly corresponding to areas of circular canopies with radius of one and two meters.

The results of pixel- and segmentation-based approaches were compared with the reference tree cover layer to evaluate the most accurate method. The index used was ExGR while the threshold was Otsu following results from sections 3.1.2 and 3.1.3.

3.1.5. Noise reduction, pale/dark objects

Salt and pepper noise elimination was based on the application of two morphological operators with a 3×3 kernel over the classified raster, where 1 marks 'tree' pixels and 0 the background. First 'Opening' was applied (erosion followed by dilation) to eliminate small segments, followed by 'Closing' (dilation followed by erosion) to eliminating small gaps (Olaya, 2016).

Abnormal objects (dark/pale) filtering was based on an illumination condition aimed at avoiding errors caused by the presence of water ponds that appear as black or white patches (specular reflection). The condition was applied by creating an illumination layer (the sum of the RGB bands), and considering as 'valid' values those within two standard deviations from the mean value of the layer. An 'invalid' mask was created this way, marking as 1 the pixels the pixels not meeting the illumination condition and the rest of them as 0. Afterwards, 'opening' was applied, followed by 'closing', both with a 3×3 kernel. Then, segments are labelled, and their areas are calculated, keeping only those that are bigger than 200 m^2 (minimum pond size over all sites). After creating this mask, it is applied as a condition after the classification, so pixels marked as 'tree' only can be considered as such if they have not been marked as 'invalid'.

3.1.6. Selected workflow

The experiments performed in the sections 3.1.2 to 3.1.5 provided a base for a final workflow to be applied to all sites. The workflow used the Otsu threshold applied to the ExGR index at pixel level as follows: 1) the ExGR index is calculated and the Ostu threshold is applied to obtain a binary image, 2) the morphological operators are applied over the image to reduce the salt-and-pepper noise and 3) dark or pale objects are eliminated (Figure 2).

3.2. FCC extraction with LiDAR

The ALS-based layers used for FCC extraction (i.e. CHM) were generated with the same spatial extent and resolution as the orthophotos. The first step, when generating the ALS-based layers, was the creation of a no-data mask in areas without LiDAR returns (i.e., water ponds). The mask was created by calculating the distance between returns and imposing a maximum distance threshold. The PNOA LiDAR data have a minimum density of 0.5 points/m^2 (IGN, 2014), which translates into a horizontal distance of approximately 1.4 m between each pair of points. Therefore, a threshold of 1.5 m was selected to mask areas without LiDAR returns. To avoid false alarms caused by variations of flight parameters (e.g., airplane roll, yaw and pitch) an area condition was also applied, (i.e., no-data zones must have a minimum area of 200 m^2). The two conditions were needed to avoid discarding small zones with larger than nominal point spacing created by platform movement and not by the presence of surface water.

Subsequently, digital elevation and digital surface models (DEM and DSM) were created using bilinear spline interpolation with Tykhonov regularization (Brovelli *et al.,* 2016). Returns classified as ground (class '2', ASPRS, 2013) were used to generate the DEM. The classification of returns was carried out by IGN and was available in the downloaded LiDAR tiles. The DSM was generated after filtering outliers, i.e., first returns with height above a reference surface (Brovelli *et al.,* 2014) bigger than 15 meters. The DEM and DSM were masked using the no-data mask. By subtracting the DEM from the DSM, the canopy height model (CHM) was obtained. A minimum height condition (2.5 m) was applied over the CHM to delineate pixels with tree cover since, as per local management practices, trees need to have a minimum height of 2 m. To avoid possible commission errors caused by ALS measurement errors (vertical RMSE of 20 cm (IGN, 2014)) the threshold was increased to 2.5 m. Every segment classified as tree (based on height) had to satisfy a second condition regarding a minimum area of 3.35 m^2 (i.e., corresponding to a circular canopy with a diameter of 1 m). The condition was imposed to discard small areas that may not belong to a tree canopy (e.g., the highest part of bushes).

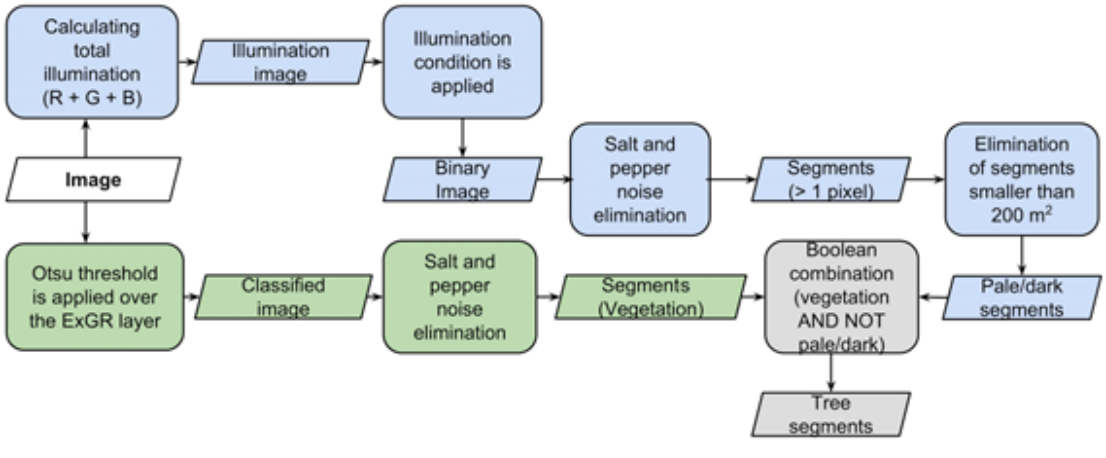

Figure 2. Workflow for the classification of tree cover using RGB images.

3.3. FCC extraction with spectral indices and ALS

The extraction of the FCC from ALS-derived metrics and RGB indices was performed using a boolean combination of a height condition (i.e. CHM over 2.5 m) and a greenness condition (ExGR of the segment above the mean value of ExGR for the entire image). The greenness threshold was selected because it showed the least omission error in earlier experiments (section 3.1), and combining it with the results obtained from LiDAR data should avoid commission errors. Both conditions were applied at pixel level. The morphologic operation 'opening' was performed to delete the small segments followed by 'closing', to avoid holes in the tree segments. Both were applied with a 3×3 kernel to eliminate the salt-and-pepper noise.

3.4. Accuracy Assessment

Reference layers for assessing the quality of the classification results were created through ortho-photo interpretation for each site. These layers are referred to as "tree presence point layer", as opposed to the canopy area layer generated for one site (i.e. CO 01) as described in section 3.1.1. Five clusters of points were placed over each orthophoto (Figure 3). Each cluster consisted of 6400 sampling points for a total of 32000 points per site. At each sampling point, the presence/absence of tree type vegetation was assessed visually. Zones with no LiDAR data in sites UP 10 and CO 06 (files not provided or coverage absent in the original file) were ignored when generating the reference layers. In this case the results were assessed using the percentages of accurate predictions, and the percentages of omission and commission errors.

4. Results

4.1. FCC extraction with RGB Indices

The spectral index showing the highest overall accuracy (89.7%) was ExGR although the difference was marginal when compared to ExG (89.2%) and CIVE (89.4%). Nevertheless, for the ExGR index segments statistics (number, mean, and median) were closest when compared to those of the reference tree cover layer (Table 2) and showed the least salt-and-pepper noise. It is important to notice the impact of the

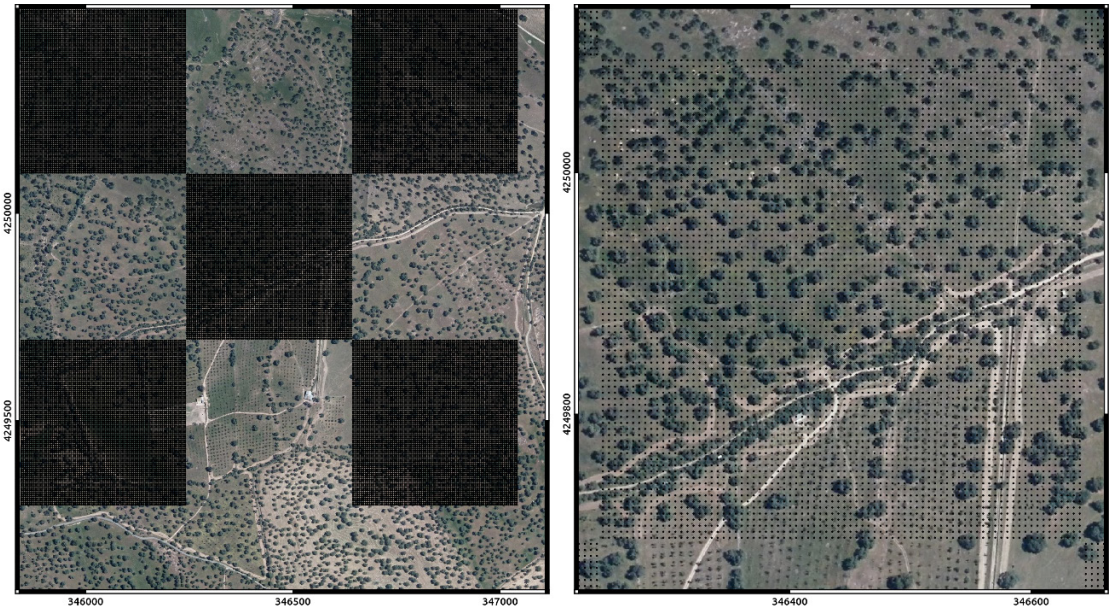

Figure 3. The five clusters of points (left panel) digitized over the site FA 05. The right panel shows central cluster. This point layer was created to assess the results.

salt-and-pepper noise on the classification accuracy. When a significant number of segments (>40%) have only one pixel, some of the accuracy indicators in Table 2 showed large discrepancies with respect to the canopy area reference layer.

Table 2. Accuracy indicators for the different RGB indices evaluated (site CO 01). ExG is the excess green index, ExGR is the excess green minus excess red and CIVE is the color index of vegetation extraction.

	ExG	ExGR	CIVE	Reference layer
Overall accuracy (%)	89.2	89.7	89.4	N/A
Omission (%)	5.4	5.1	6.0	N/A
Commission (%)	5.4	5.2	4.7	N/A
Segments (n)	7494	4200	6706	1967
N° of segments over 1 pixel	3538	2436	3288	N/A
Mean (m^2)	23.8	42.8	24.8	91.6
Median (m^2)	0.25	0.74	0.25	52.5

The Otsu threshold allowed for the highest overall accuracy while also balancing omission and commission errors. The remaining thresholding methods showed a strong tendency towards omission ('0' value threshold) and respectively commission (mean value threshold) errors (Table 3). It is important to notice that using the mean ExGR as threshold provided segments of similar size and number when compared to those observed for the canopy area reference layer. However, the commission errors were above 15% when compared to the 5% when using the Otsu threshold.

Table 3. Accuracy results for the different thresholds evaluated (site CO 01).

	0 value	Mean ExGR	Otsu	Reference layer
Overall accuracy (%)	85.8	83.4	89.7	N/A
Omission (%)	13.4	1.2	5.1	N/A
Commission (%)	0.8	15.4	5.2	N/A
Segments (n)	7036	2563	4200	1967
N° of segments over 1 pixel	3623	868	2436	N/A
Mean (m^2)	7.4	80.6	42.8	91.6
Median (m^2)	0.49	0.748	0.74	52.5

Regarding the segmentation approach, using simple thresholding at pixel level resulted in the highest overall accuracy (89.7%) although only marginally above the accuracy obtained using region-growing techniques (i.e. 1%). The number of segments for the region-growing approach was lower while the mean segment size was higher when compared to the canopy area reference layer (48%) showing that many small segments were omitted (Table 4). Considering all indicators, the pixel-level thresholding approach was considered better suited for tree cover classification.

After the application of the morphological operators the overall accuracy decreased slightly although a slight increase of omission error was also noticed. However, the commission error decreased, and the number of patches and their average size were significantly closer when compared to those observed for the canopy area reference layer (Table 4). As such, it was considered that morphological operators provide significant improvements on tree cover

Table 4. Accuracy indicators for different segmentation approaches and corrections.

	Segmentation		Morphologic operators		Illumination Condition applied	Reference Layer
	Region Growing	Pixel level	No Correction	Corrected		
Overall accuracy (%)	88.8	89.7	89.7	89.7	89.0	N/A
Omission (%)	4.5	5.1	5.1	5.3	5.30	N/A
Comm. (%)	6.6	5.2	5.2	5.0	5.76	N/A
Segments (n)	1246	4200	4200	1845	1788	1967
Mean (m^2)	160.1	42.8	42.8	95.3	102.1	91.6
Median (m^2)	72.59	0.74	0.74	33.42	36.00	52.5

Table 5. Accuracy results after applying the RGB, LiDAR and combined approaches.

	Overall accuracy			Omission error			Commission error		
Site	RGB	ALS	RGB+ALS	RGB	ALS	RGB+ALS	RGB	ALS	RGB+ALS
UP 10 2008	93	93	94	6	6	5	1	1	1
UP 10 2013	55			3			42		
CO 06	83	90	86	9	8	13	8	2	1
AS 07	82	80	80	10	16	18	8	4	2
AP 06	84	89	89	10	7	9	5	4	2
AS 02	73	88	89	5	7	9	22	4	2
AS 06	74	82	83	9	10	13	15	8	4
FA 05	75	85	85	10	11	13	15	4	2
UP 24	88	91	90	7	8	9	5	1	1
CO 01	90	92	94	6	2	3	4	6	3
UP 07	80	84	85	7	10	11	13	6	4

classification and were therefore incorporated into the final workflow (Figure 2).

Pale and dark objects elimination slightly lowered the overall accuracy while the number of segments and segment indicated omission of small segments. However, visual inspection showed that open water areas were correctly eliminated.

Using the final workflow, the overall accuracy over all sites reached 82.5±10% (mean and standard deviation). When looking at individual sites the overall accuracy varied between 55% and 93% (Table 5). Notice that, in Table 5, the two orthophotos available for site UP 10 (2008, 2013) have been treated separately.

Tree canopies over bare ground were detected with low commission errors but omission errors for canopy borders and small canopies were observed. All sites with a 15% or more commission error (UP 10 2013, AS 02, AS 06 and FA 05) showed abundant presence of green pastures and shrubs. This is particularly noticeable for site UP 10 over the two orthophotos taken at different dates (Figure 4). Whereas the results obtained for the 2008 orthophoto were the most accurate (93%), those obtained with 2013 orthophoto were the worst (55%) among all sites. Such discrepancies are explained by the image acquisition date. The 2008 image was acquired in September, when vegetation vigour is lower (dry summers). In such conditions the confusion between vegetation types was less problematic as trees contrasted against a background of dry grass/shrub vegetation. The opposite was true for the 2013 image acquired in June.

4.2. FCC extraction with LiDAR

LiDAR based FCC extraction achieved an overall accuracy of 87±4% over all sites (Table 5) with values of individual sites varying between 80 and 93%. Upon visual inspection, the results obtained were satisfactory. However, small commission errors were still present, mostly related to areas of close canopies and their borders. Such errors may be attributed to the CHM interpolation, whose results are very smooth, causing canopies to i) 'fade' into the background as distance from center increases and ii) 'fusing' canopies or buildings that are closely spaced. The water bodies and ponds have been removed correctly using the LiDAR approach, except for a small patch of the dam separating parts of site UP 24.

It is important to mention that the original LiDAR data had some errors. The most relevant was point classification accuracy in areas with steep slopes or a thick shrubs layer where points were wrongly classified as vegetation and ground, respectively. Additional errors were caused by differences in the height retrieved from adjacent scan lines (although they only appear at three sites). These errors were observed using a hill shaded terrain layer, obtained from the DEM. Such differences were small, about 20 cm, and thus within the flight parameters and were not observed in the hill shaded layer produced from the CHM.

When compared to optical based indices, the classification accuracy increased for most sites when using just ALS data, despite of the unsophisticated method implemented. On average, the overall accuracy increased by 8% with the biggest

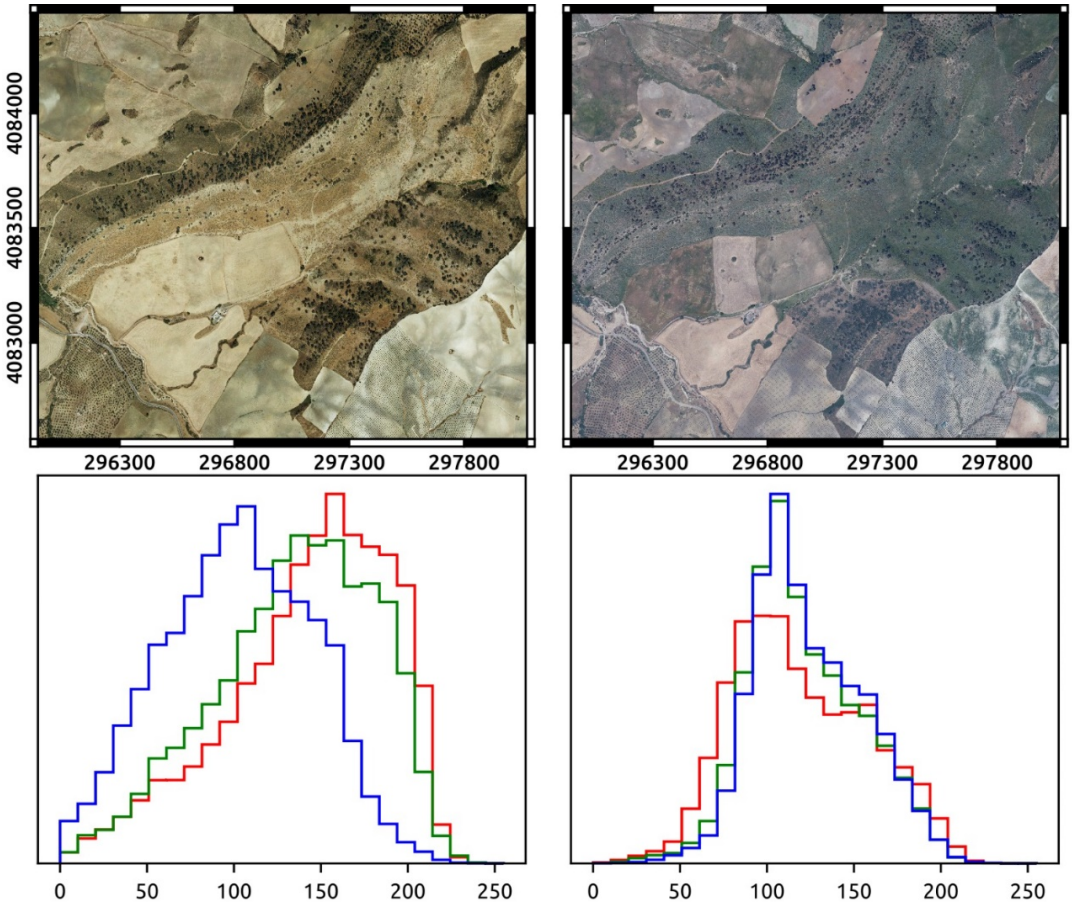

Figure 4. Orthophotos of the site UP 10 from September of 2008 (left) and June of 2013 (right) and the histogram of each of the channels of the image (RGB).

increase (38%) being observed for the site UP 10 2013. Such a large difference was explained by the abundance of vigorous non-tree vegetation (i.e. pasture), which caused confusion when using the RGB indices alone highlighting the need of timing airborne acquisitions during dryer periods when the objective is FCC extraction. Conversely, in some sites there was no improvement in the accuracy when using the ALS data since the aerial imagery was acquired during periods when grasses and shrubs were dry. (e.g. UP 10 when using the airborne image acquired in 2008). Finally, lower accuracies (about 2%) were observed when using the ALS data for site AS 07. This was linked to the steep slopes of the area, which caused errors in the classification of LiDAR returns, and thus, in the canopy height model used for classification. Such variations demonstrated that the use of ALS data might not provide more accurate results over the entire landscape.

4.3. FCC extraction with RGB indices and LiDAR

Using both LiDAR and RGB indices, the overall accuracy increased marginally to an average of 87.5±5% over all sites. Nevertheless, a noticeable descent of the commission error was observed (mean improvement of 1.5%, maximum improvement of 4%). Table 5 shows the results of the accuracy assessment for the combined used of spectral indices and ALS derived metrics. The overall accuracy varied between 80 and 94% with the largest omission errors being observed for site AS 07. Commission errors were below 5% for all sites. Visual inspection of the results

showed that the delineation of canopies improved. Unfortunately, omission errors also increased since canopy borders and many small canopies were not extracted. The errors were caused by the thresholding method which appeared to set a too high value. Even when using the mean of the ExGR layer as threshold (less prone to omission errors, section 4.1) the omission errors persisted.

5. Discussion

The results obtained were acceptable for most combinations of algorithms and sites, with just 3 tests out of 31 with an accuracy below 75%. These three cases appeared when using the approach based on thresholding of the RGB indices, where the commission error was equal or over 15%. Note that when comparing the results obtained by the different algorithms, LiDAR-based solutions where able to achieve lower commission errors, thanks to their ability to separate different types of vegetation by height, whereas, depending on the period, greenness can be a common characteristic of pasture, shrub and tree strata. When both LiDAR and RGB information were combined, the commission error decreases even further, showing the critical role of the ALS information content. The results obtained using RGB indices contrast with those obtained by Castillejo-González *et al.* (2010), who reported a 90% of accuracy using Quickbird images. It seems, they were able to improve accuracy metrics by incorporating the NDVI along with the RGB and near infrared bands (NIR). Romero de los Reyes *et al.* (2007) and Lavado *et al.* (2012) used similar methods and data to the ones presented in section 3.1 (thresholding and OBIA, respectively), but they did not mention the accuracy of the results obtained which precludes an objective comparison. In most cases imagery acquired during the dry season is employed to increase the contrast between pastures and tree strata (Pu *et al.,* 2003; Xu *et al.,* 2003; Boggs, 2010; Abbasi & Bakhtyari, 2012). Joffre and Lacaze (1993) and Castillejo-González *et al.* (2010) used imagery acquired during April, although the latter recommends using summer imagery, when pasture is dry. In the case of shrubs, the most common approach to avoid confounding effects is to mask them (Ke & Quackenbush, 2011). For example Romero de los Reyes *et al.* (2007) eluded this problem completely by not selecting *dehesas* with presence of shrubs.

Omission errors related to canopy borders and/or small trees could be attributed to the decrease of contrast between canopies and background when using coarser pixel sizes (Fernández de Ahumada & Martínez-Ruedas, 2017). Boggs (2010) mentions similar effects in some of his experiments, where NDVI thresholding produced different number of different sized segments depending on the sensor employed. When using higher resolution imagery (Quickbird), the segments were smaller and more numerous, whereas the contrary happened when using coarser resolution images (i.e. SPOT 5), where the canopies delineated were fewer and bigger. Such effects provide a possible explanation for the results described in section 4.1, i.e. small trees and canopy borders might have values nearer to the background values, which causes them to fall under the greenness threshold, whereas small trees may be grouped with 'ground' segments, having little effect on the segment overall greenness, and thus, they are omitted.

The LiDAR-based approach was mainly affected by errors related to errors in the original point cloud, the interpolation process or both. Point cloud-related errors are linked to the loose co-registration of adjacent flight lines, and misclassification of returns, which caused canopy height to be underestimated over steeply sloped areas. Interpolation errors were caused by the low density of the LiDAR point cloud and the selected interpolation method. The land surfaces are sparsely sampled by the PNOS LiDAR, thus, both the canopy top (maximum height) and borders might be missed (Zimble *et al.,* 2003). When this sparse point cloud is passed to the interpolation algorithm it lacks important breakpoints and thus the CHM is created disregarding them. This can cause the canopy border height to be under- or overestimated due to canopy 'fusing' and 'fading' (section 4.2.). Each of these problems may be solved with specific solutions. The wavy pattern caused by adjacent flight lines can be solved by sampling the original data (i.e. Poisson sampling, Butler and Gerlek, 2017), whereas using a different algorithm for point classification might improve the results, for example, the multiscale curvature algorithm (Evans & Hudak, 2007).

The combined LiDAR-optical based approach did not significantly increase the overall accuracy but reduced commission errors. Visual inspection showed that canopies delineation has improved, although canopy borders or small canopies were likely to be omitted. Chen *et al.* (2005) report 88% accuracy in tree counting (canopies correctly detected) using higher resolution orthophotos (10 cm) as well as point clouds with a mean density of at least 1.6 points/m^2. Mumtaz and Mooney (2008) and Dechesne *et al.* (2016) reported accuracies above 90% (94 and 99%) for tree extraction in similar environments. However, these studies used very high resolution (15 to 50 cm) multispectral images and significantly denser point clouds (2 to 3 points/m^2). Notice that a band dedicated to Near Infrared was available for both, so it was possible to calculate the NDVI, which played a crucial role when extracting the tree cover (Mumtaz & Mooney, 2008). Since higher resolution data sets are not readily collected, the high accuracies reported are not easy to replicate over large areas over which one should expect more moderate estimates (around 80%) when using regional or national datasets.

6. Conclusions

This study focused on determining which sensors (i.e., optical *vs.* LiDAR) and techniques (spectral indices, thresholding, and segmentation) are optimal for tree cover extraction in *dehesas*. The results showed that RGB-based techniques may attain accurate results. However, optical based extraction is vulnerable to confusion between trees and shrubs or vigorous pastures as well as small omission errors related to the spatial resolution. LiDAR provided higher accuracies benefitting significantly from height information. However, ALS based techniques were hindered by the low point cloud density and point classification errors. The most accurate results were obtained by combining RGB and LiDAR metrics although the increase in accuracy was rather small when compared to using ALS or optical data alone.

Extracting tree cover from orthophotos resulted in reasonable accuracies (80%). However, the commission errors caused by the presence of low vegetation, ponds, and roads were relatively high. When there was a strong contrast between tree canopies and the background, the use of optical indices provided overall accuracies above 90%. The relatively small increase in the overall accuracy (8%) when adding ALS data, the lower temporal frequency of ALS acquisitions (orthophotos are taken every 2-3 years, whereas ALS data only have been collected once) and the existence of data from historical campaigns (IGN, 2014) underline the utility of the existing optical archives to both, update tree cover information and retrieve its historical levels, a valuable information for long-term studies.

Acknowledgments

IGN and the Andalusian government are acknowledged for providing the airborne datasets. The study was carried out under the projects LIFE+ bioDehesa (LIFE11/BIO/ES/000726) and FUNDIVER (MINECO, Spain; CGL2015-69186-C2-2-R projects), funded through the LIFE+ program.

References

Abbasi, M., Bakhtyari, H.R. 2012. Extraction of Forest Stands Parameters from Aster Data in Open Forest. *International Archives of the Photogrammetry, Remote Sensing and Spatial Information Sciences*, *39*, B4. https://doi.org/10.5194/isprsarchives-XXXIX-B4-153-2012

ASPRS, American Society of Photogrammetry and remote sensing. 2013. *LAS specification version 1.4 – R13*. Retrieved from https://www.asprs.org/wp-content/uploads/2010/12/LAS_1_4_r13.pdf Last access: June 2019.

Boggs, G.S. 2010. Assessment of SPOT 5 and QuickBird remotely sensed imagery for mapping tree cover in savannas. *International Journal of Applied Earth Observation and Geoinformation*, *12*(4), 217-224. https://doi.org/10.1016/j.jag.2009.11.001

Brovelli, M.A., Cannata, M., Longoni, U., Reguzzoni, M., Antolin, R. 2014. *v.outlier, removes outliers from vector point data* [English]. Retrieved from https://grass.osgeo.org/grass72/manuals/v.outlier.html Last access: June 2019.

Brovelli, M.A., Cannata, M., Longoni, U., Reguzzoni, M., Antolin, R. 2016. *GRASS GIS manual: v.surf.bspline* [English]. Retrieved from https://grass.osgeo.org/grass72/manuals/v.surf.bspline.html Last access: June 2019.

Butler, H., Gerlek, M. 2017. *PDAL Point Data Abstraction Library* [English]. Retrieved from https://www.pdal.io Last access: June 2019.

Carreiras, J.M., Pereira, J.M., Pereira, J.S. 2006. Estimation of tree canopy cover in evergreen oak woodlands using remote sensing. *Forest Ecology and Management*, *223*(1-3), 45-53. https://doi.org/10.1016/j.foreco.2005.10.056

Castillejo-González, I.L., Guerrero, J.M.M., García-Ferrer Porras, A., F.J. Mesas-Carrascosa, M.S. de la O. 2010. Utilización de imágenes de satélite de alta resolución espacial en la determinación de la fracción de cabida cubierta en sistemas adehesados. In Ojeda, J., Pita, M.F. y Vallejo, I. (Ed.), *XIV Congreso nacional de Tecnologías de la Información Geográfica. La Información Geográfica al Servicio de los Ciudadanos: de lo Global a lo Local* (pp. 62-71). Secretariado de Publicaciones de la Universidad de Sevilla.

Chen, L., Chiang, T., Teo, T. 2005. Fusion of LIDAR data and high-resolution images for forest canopy modelling. *Proc. 26th Asian Conference on Remote Sensing*.

De Miguel, J.M., Acosta-Gallo, B., Gómez-Sal, A. 2013. Understanding mediterranean pasture dynamics: general tree cover *vs.* specific effects of individual trees. *Rangeland Ecology & Management*, *66*(2), 216-223. https://doi.org/10.2111/REM-D-12-00016.1

Dechesne, C., Mallet, C., Bris, A.L., Gouet, V., Hervieu, A. 2016. Forest Stand Segmentation Using Airborne Lidar Data and Very High Resolution Multispectral Imagery. *ISPRS - International Archives of the Photogrammetry, Remote Sensing and Spatial Information Sciences*, *XLI-B3*, 207–214. https://doi.org/10.5194/isprs-archives-xli-b3-207-2016

Evans, J.S., Hudak, A.T. 2007. A Multiscale Curvature Algorithm for Classifying Discrete Return LiDAR in Forested Environments. *IEEE Transactions on Geoscience and Remote Sensing*, *45*(4), 1029-1038. https://doi.org/10.1109/tgrs.2006.890412

Fernández de Ahumada, E., Martínez-Ruedas, C. 2017. El análisis de imagen como herramienta para la cuantificación del número de árboles y La fracción de cabida cubierta en sistemas agrosilvopastorales. Retrieved from http://www.uco.es/investigacion/proyectos/biodehesa/wp-content/uploads/An%C3%A1lisis_imagen_herramienta_cuantificaci%C3%B3n_n%C2%BA%C3%A1rboles_FCC_St%C2%AAagrosilvopastorales.pdf Last access: June 2019.

Fisher, A., Day, M., Gill, T., Roff, A., Danaher, T., & Flood, N. 2016. Large-area, high-resolution tree cover mapping with multi-temporal SPOT5 imagery, New South Wales, Australia. *Remote Sensing*, *8*(6), 515. https://doi.org/10.3390/rs8060515

Free Software Foundation. 2016. gnu.org. Retrieved from https://www.gnu.org/philosophy/free-sw.html Last access: June 2019.

García, M. 2011. *Obtención de variables forestales a partir de datos lidar* (p. 16). Retrieved from Ministerio de Agricultura, Alimentación y Medio Ambiente; Red nacional de parques naturales; Tragsatec: https://www.miteco.gob.es/es/parques-nacionales-oapn/plan-seguimiento-evaluacion/documento-tecnico-obtencion-variables-lidar_tcm30-68999.pdf Last access: June 2019.

Godinho, S., Guiomar, N., Gil, A. 2018. Estimating tree canopy cover percentage in a mediterranean silvopastoral systems using Sentinel-2A imagery and the stochastic gradient boosting algorithm. *International Journal of Remote Sensing*, *39*(14), 4640-4662. https://doi.org/10.1080/01431161.2017.1399480

Gómez-Sal, A., Velado Alonso, E., González-García, A. 2016. *Tipología y caracterización de las dehesas del proyecto LIFE+ bioDehesa para la representación de dehesas representativas*. Retrieved from http://www.uco.es/investigacion/proyectos/biodehesa/wp-content/uploads/Informe_2_Caracterizaci%C3%B3n_fincas_RDD_II.pdf Last access: June 2019.

Guijarro, M., Pajares, G., Riomoros, I., Herrera, P. J., Burgos-Artizzu, X.P., Ribeiro, A. 2011. Automatic segmentation of relevant textures in agricultural images. *Computers and Electronics in Agriculture*, *75*(1), 75-83. https://doi.org/10.1016/j.compag.2010.09.013

IGN, Instituto Geográfico Nacional. 2014. National Plan for Aerial Orthophotography. Retrieved May 21, 2019, from http://pnoa.ign.es/ .

IGN, Instituto Geográfico Nacional. 2016. Plan Nacional de Ortofotografía Aérea. Especificaciones técnicas. Retrieved May 21, 2019, from http://pnoa.ign.es/caracteristicas-tecnicas

IGN, Instituto Geográfico Nacional. 2019. Especificaciones Técnicas para vuelo LiDAR y procesado del MDE.

Inglada, J., Christophe, E. 2009. The Orfeo Toolbox remote sensing image processing software. *2009 IEEE International Geoscience and Remote Sensing Symposium*. https://doi.org/10.1109/igarss.2009.5417481

Jennings, S., Brown, N., Sheil, D. 1999. Assessing forest canopies and understorey illumination: canopy closure, canopy cover and other measures. *Forestry: An International Journal of Forest Research*, *72*(1), 59-74. https://doi.org/10.1093/forestry/72.1.59

Joffre, R., Lacaze, B. 1993. Estimating tree density in oak savanna-like 'dehesa' of southern Spain from SPOT data. *International Journal of Remote Sensing*, *14*(4), 685-697. https://doi.org/10.1080/01431169308904368

Jones, E., Oliphant, T., Peterson, P. 2014. *SciPy: Open source scientific tools for Python*.

Jones, H.G., Vaughan, R.A. 2010. *Remote Sensing of Vegetation*. Oxford University Press.

Junta de Andalucía. (2018, February 7). Distribución de las formaciones adehesadas en Andalucía, información actualizada. Retrieved April 4, 2019, from https://laboratoriorediam.cica.es/geonetwork/srv/esp/metadata.show?currTab=simple&id=19762

Kataoka, T., Kaneko, T., Okamoto, H., Hata, S. 2003. Crop growth estimation system using machine vision. *Proceedings 2003 IEEE/ASME International Conference on Advanced Intelligent Mechatronics (AIM 2003)*. https://doi.org/10.1109/aim.2003.1225492

Ke, Y., Quackenbush, L.J. 2011. A review of methods for automatic individual tree-crown detection and delineation from passive remote sensing. *International Journal of Remote Sensing*, *32*(17), 4725-4747. https://doi.org/10.1080/01431161.2010.494184

Lavado, J.F., Jariego, A., Schnabel, S., Gómez, A. 2012. Análisis de la evolución histórica del arbolado de la dehesa mediante fotointerpretación y análisis OBIA. In J. Martínez Vega & P. Martín Isabel (Eds.), *XV Congreso Nacional de Tecnologías de la Información Geográfica. Tecnologías de Información Geográfica en el contexto de Cambio Global* (pp. 92-100). CSIC-Instituto de Economía, Geografía y Demografía (IEGD).

Lennert, M. 2016. *i.segment.uspo, unsupervised segmentation parameter optimization for i.segment* [English]. Retrieved from https://grass.osgeo.org/grass70/manuals/addons/i.segment.uspo.html Last access: June 2019.

McGaughey, R.J. 2016. *FUSION/LDV: Software for LIDAR data analysis and visualization* [English]. USDA Forest Service.

Meyer, G.E., Hindman, T.W., Laksmi, K. 1999. Machine vision detection parameters for plant species identification. In G.E. Meyer & J.A. DeShazer (Eds.), *Precision Agriculture and Biological Quality*. https://doi.org/10.1117/12.336896

Meyer, G.E., Neto, J.C. 2008. Verification of color vegetation indices for automated crop imaging applications. *Computers and Electronics in Agriculture*, *63*(2), 282-293. https://doi.org/10.1016/j.compag.2008.03.009

Moreno, G., Pulido, F.J. 2009. The Functioning, Management and Persistence of Dehesas. In A. Rigueiro-Rodríguez, J. McAdam, & M.R. Mosquera-Losada (Eds.), *Agroforestry in Europe: Current Status and Future Prospects* (pp. 127-160). https://doi.org/10.1007/978-1-4020-8272-6_7

Morsdorf, F., Kötz, B., Meier, E., Itten, K.I., Allgöwer, B. 2006. Estimation of LAI and fractional cover from small footprint airborne laser scanning data based on gap fraction. *Remote Sensing of Environment*, *104*(1), 50-61. https://doi.org/10.1016/j.rse.2006.04.019

Mumtaz, S.A., Mooney, K. 2008. Fusion of high resolution lidar and aerial images for object extraction. *2nd International Conference on Advances in Space Technologies*. https://doi.org/10.1109/icast.2008.4747701

Neteler, M., Mitasova, H. (Eds.). 2008. *Open Source GIS: A GRASS GIS Approach*. https://doi.org/10.1007/978-0-387-68574-8

Olaya, V. 2016. *Sistemas de información geográfica*.

Otsu, N. 1979. A Threshold Selection Method from Gray-Level Histograms. *IEEE Trans. Syst. Man Cybern.*, *9*(1), 62-66. https://doi.org/10.1109/TSMC.1979.4310076

Pu, R., Xu, B., Gong, P. 2003. Oakwood crown closure estimation by unmixing Landsat TM data. *International Journal of Remote Sensing*, *24*(22), 4422-4445. https://doi.org/10.1080/0143116031000095989

Python Software Foundation. 2010. *Python language reference, version 2.7*. Python Software Foundation.

Quantum GIS Development Team. 2017. *QGIS* [English]. Retrieved from https://www.qgis.org/en/site/ Last access: June 2019.

Romero de los Reyes, E., Navarro Cerrillo, R., García-Ferrer, A. 2007. Aplicación de ortofotos para la estimación de pérdida de individuos en dehesas de encina: ("Quercus ilex" L. subps. "ballota" (Desf.) Samp.) afectadas por procesos de decaimiento. *Boletín de sanidad vegetal. Plagas.*, *33*(1), 121-134.

Soininen, A., & TerraSolid. 2016. *TerraScan Users' Guide*.

van der Walt, S., Colbert, S.C., Varoquaux, G. 2011. The NumPy Array: A Structure for Efficient Numerical Computation. *Computing in Science & Engineering*, *13*(2),22–30.https://doi.org/10.1109/MCSE.2011.37

van der Walt, S., Schönberger, J. L., Nunez-Iglesias, J., Boulogne, F., Warner, J. D., Yager, N., … Yu, T. 2014. scikit-image: image processing in Python. *PeerJ*, *2*, e453. https://doi.org/10.7717/peerj.453

White, MA., Asner, G.P., Nemani, R.R., Privette, J.L., Running, S.W. 2000. Measuring Fractional Cover and Leaf Area Index in Arid Ecosystems. *Remote Sensing of Environment*, *74*(1), 45-57. https://doi.org/10.1016/s0034-4257(00)00119-x

Woebbecke, D.M., Meyer, G.E., Von Bargen, K., Mortensen, D.A. 1995. Color Indices for Weed Identification Under Various Soil, Residue, and Lighting Conditions. *Transactions of the ASAE*, *38*(1), 259. https://doi.org/10.13031/2013.27838

Xu, B., Gong, P., Pu, R. 2003. Crown closure estimation of oak savannah in a dry season with Landsat TM imagery: comparison of various indices through correlation analysis. *International Journal of Remote Sensing*, *24*(9), 1811-1822. https://doi.org/10.1080/01431160210144598

Zimble, D.A., Evans, D.L., Carlson, G.C., Parker, R.C., Grado, S.C., Gerard, P.D. 2003. Characterizing vertical forest structure using small-footprint airborne LiDAR. *Remote Sensing of Environment*, *87*(2-3), 171-182. https://doi.org/10.1016/S0034-4257(03)00139-1